

Rupture of thin liquid films: Generalization of weakly nonlinear theory

B. Y. Rubinstein¹ and A. M. Leshansky^{2,*}

¹*Stowers Institute for Medical Research, 1000 E. 50th St., Kansas City, Missouri 64110, USA*

²*Department of Chemical Engineering, Technion–IIT, Haifa, IL-32000, Israel*

(Received 1 August 2010; published 21 March 2011)

In this paper, we investigate the rupture dynamics of thin liquid films driven by intermolecular forces via weakly nonlinear bifurcation analysis. The dynamic equations governing slow dynamics of the perturbation amplitude of the near-critical mode corresponding to several models describing the evolution of thin liquid films in different physical situations appear to have the same structure. When antagonistic (attractive and repulsive) molecular forces are considered, nonlinear saturation of the instability becomes possible, while the boundary of this supercritical bifurcation is determined solely by the form of the intermolecular potential. The rupture time estimate obtained in closed form shows an excellent agreement with the results of the previously reported numerical simulations of the strongly nonlinear coupled evolution equations upon fitting the amplitude of the small initial perturbation. We further extend the weakly nonlinear analysis of the film dynamics and apply the Galerkin approximation to derive the amplitude equation(s) governing the dynamics of the fastest growing linear mode far from the instability threshold. The comparison of the rupture time derived from this theory with the results of numerical simulations of the original nonlinear evolution equations shows a very good agreement without any adjustable parameters.

DOI: [10.1103/PhysRevE.83.031603](https://doi.org/10.1103/PhysRevE.83.031603)

PACS number(s): 68.15.+e, 47.15.gm, 47.20.Ky, 68.08.–p

I. INTRODUCTION

It is well known that a liquid film on a planar solid surface may become unstable due to long-range molecular forces. The forces originating from van der Waals attractions [1] accelerate thinning in regions of film depression leading to film rupture and subsequent dewetting [2]. On the other hand, electrical double layers on the solid surface may give rise to intermolecular repulsions stabilizing thin films against rupture [3].

In recent years, much effort has been put into theoretical modeling of the dewetting phenomena [4–13]. A nonlinear theory of the film evolution based on the long-wave nature of the response was first proposed in Ref. [4]. This approach, which has already been considered for different situations [5], yields nonlinear partial differential equations that describe the evolution of the interface shape, surfactant concentration, tangential liquid velocity, and others. Linear stability analysis is routinely applied to predict the onset of the instability and the characteristic wavelength. The general feature of the van der Waals–driven instability is that, for small wave numbers k , the perturbation growth rate $\sigma(k) \approx \alpha k^2 + \beta k^4 + \dots$, where α and β are functions of the relevant governing parameters. The quadratic term may change sign, while the $\mathcal{O}(k^4)$ term is negative reflecting the stabilizing action of the surface tension. Therefore, for the positive values of α , there is a critical (or cutoff) wave number k_c , such that $\sigma(k_c) = 0$ and $\sigma(k) > 0$ for $0 < k < k_c$. Also, the dispersion curve $\sigma(k)$ reaches a maximum σ_m at some k_m , such that $0 < k_m < k_c$. The rupture time can be estimated assuming that small initial perturbation in the film thickness $\tilde{h} \ll h_0$ grows exponentially with the time rate σ_m giving $t_{\text{rup}} \sim -\sigma_m^{-1} \ln(\tilde{h}/h_0)$, where h_0 is the initial thickness. The prediction of the linear theory turns out to be rather poor: it usually overestimates the

rupture time due to the highly nonlinear nature of the rupture process driven by intermolecular forces. The most common and straightforward approach is to solve the original evolution equation(s) numerically [6–8, 10–12, 14, 15] and determine the rupture time as the film thickness reaches the critical value of, say, 0.1% of the initial thickness. The obvious disadvantage of the numerical simulation is that, for a complex problem that involves many parameters, the full parametric study of rupture is quite elaborate.

A bifurcation technique was first applied in [13] to arrive at the nonlinear estimate for the rupture time in the vicinity of a bifurcation point corresponding to $\sigma(k_c) = 0$. It was demonstrated that nonlinear terms owing to van der Waals attractions contribute to rapid acceleration of the rupture beyond the linear regime. Analysis of the nonlinear evolution of small disturbances leads to a dynamic Landau equation for the perturbation amplitude. The closed-form solution of the amplitude equation that provides a value of the finite blowup time of the initial small-amplitude disturbance was proposed to be a good estimate of the nonlinear rupture time [9, 13]. In other words, the weakly nonlinear theory predicts a sudden and rapid change of the perturbation amplitude at some finite time, while the linear stability analysis suggests the gradual (exponential) change in perturbation amplitude. Obviously, when the perturbation amplitude becomes comparable to the film thickness, the weakly nonlinear theory, assuming small deviation from the bifurcation point, becomes formally invalid. However, the initial sudden growth of the amplitude is adequately described by the Landau equation, and the weakly nonlinear analysis is expected to yield a better description of the rupture dynamics than the linearized theory.

The approach has never been given enough attention perhaps because the derivation involves rather tedious algebra and can only be readily performed for some simple cases [16, 17]. It was demonstrated in [9], however, that the derivation of the amplitude equation can be automatized by using a previously developed symbolic algorithm for bifurcation analysis [18].

*lisha@tx.technion.ac.il

Recently, an extensive numerical investigation of the thin-film rupture driven by van der Waals attractive forces in the presence of insoluble surfactant and hydrodynamic slip was reported in [10]. In our previous paper [19], we briefly described the generalization of the theory in [9] for an arbitrary intermolecular potential. The preliminary comparison between the nonlinear theory developed in [19] for an arbitrary intermolecular potential and the numerical results corresponding to solution of the original highly nonlinear coupled evolution partial differential equations (PDEs) [10] showed a striking quantitative agreement, suggesting that the cubic nonlinearity in the resulting dynamic equation for perturbation amplitude adequately captures the underlying physics of the film rupture. Although the *qualitative* dependence of the rupture time on all governing parameters can be accurately revealed from the weakly nonlinear model, the *quantitative* agreement with the numerical results is only obtained upon fitting the amplitude of the initial disturbance. This discrepancy stems from the fact that, in simulations (and in experiments), the film rupture is controlled by the dynamics of the fastest growing mode with wave number k_m , while in [19] we examined the dynamics of the *near-critical* mode at a steady bifurcation point corresponding to the wave number k_c . More specifically, we considered the dynamics of the film in the bounded domain $0 < x \leq 2\pi/k_c$ with periodic boundary conditions, where perturbations with wave numbers less than k_c are not admissible. Nevertheless, a single value of the amplitude of the initial disturbance chosen once (in a single point in a parameter space) yields a very close agreement between the prediction of our theory and the numerical simulations upon varying other parameters. This indicates that the near-critical weakly nonlinear theory can adequately capture the underlying physics of dewetting even far from the instability threshold. However, the fact that the near-critical theory can provide the correct quantitative prediction of the rupture time only upon fitting the initial disturbance amplitude a_0 comprises the obvious disadvantage of the approach. One still needs to have a reliable estimate of t_{rup} , at least at one point in the parameter space from either experiment or simulation, to be able to perform this adjustment. Since we also do not know the relationship between the amplitude of the initial disturbances at k_c and k_m , it is not clear whether such matching of a_0 will work in general for an arbitrary system of evolution equations. To address this issue, we develop here the nonlinear theory of the film rupture at the fastest growing wavelength k_m using the Galerkin method. In this case, the theory is expected to be fully consistent with numerical simulations since it pertains to exactly the same mechanism of the film rupture via the growth of the most dangerous mode.

The organization of the paper is as follows. First, the detailed derivations of the near-critical and the nonequilibrium film-rupture theories are given in detail in Sec. II. Further, some particular examples of equations describing dynamics of thin liquid films in the long-scale approximation for different physical situations are considered in Secs. III and IV, and the rupture time estimates based on both approaches are determined and compared with available numerical results. Finally, in Sec. V, a brief summary and concluding remarks are given.

II. DERIVATION OF GOVERNING AMPLITUDE EQUATIONS

A. Critical mode case

Consider in detail the procedure of a weakly nonlinear analysis of the problem

$$\partial_t \mathbf{u} = \mathbf{f}(\nabla, \mathbf{u}, R), \quad (1)$$

assuming that a homogeneous stationary basic state \mathbf{u}_0 loses its stability at some critical value R_c of the bifurcation parameter R , and a single short-wave unstable mode with the critical wave number k_c is excited. In (1), ∂_t and ∇ denote the differentiation operators with respect to temporal t and spatial x variables, respectively; $\mathbf{u}(x, t)$ is the phase-space vector, and \mathbf{f} is the vectorial function differentiable a sufficient number of times.

The small perturbation $\tilde{\mathbf{u}}(x, t, R) = \mathcal{O}(\epsilon)$, where the small parameter $0 < \epsilon \ll 1$, of the basic solution in the linear approximation satisfies the equation

$$\partial_t \tilde{\mathbf{u}} = \mathcal{L}(\nabla, \mathbf{u}_0, R) \tilde{\mathbf{u}}, \quad (2)$$

where $\mathcal{L} = \mathbf{f}_{\mathbf{u}}$ is a linear operator calculated at the point $\mathbf{u} = \mathbf{u}_0$ and $\tilde{\mathbf{u}}$ has the form

$$\tilde{\mathbf{u}} = a\mathbf{U} \exp(ik_c x) + a^* \mathbf{U}^* \exp(-ik_c x), \quad (3)$$

where \mathbf{U} is the eigenvector of the linear problem (2) verifying the equation $\mathcal{L}\mathbf{U} = 0$ and the asterisk (*) denotes an operation of the complex conjugation.

Next, we use the expansions for variables \mathbf{u} and the bifurcation parameter R in the small parameter ϵ :

$$\begin{aligned} \mathbf{u} &= \mathbf{u}_0 + \epsilon \mathbf{u}_1 + \epsilon^2 \mathbf{u}_2 + \dots, \\ R &= R_c + \epsilon R_1 + \epsilon^2 R_2 + \dots, \end{aligned} \quad (4)$$

where R_1, R_2 are some arbitrary $\mathcal{O}(1)$ constants. We further introduce a hierarchy of time scales t_k and spatial scales x_k rescaled by the factor ϵ^k , thereby replacing the function $\mathbf{u}(x, t)$ by a function of an array of rescaled time and spatial variables. Accordingly, the time derivative is expanded in a series of partial derivatives $\partial_k \equiv \partial/\partial t_k$:

$$\partial_t = \partial_0 + \epsilon \partial_1 + \epsilon^2 \partial_2 + \dots. \quad (5)$$

The spatial derivative is expanded similarly:

$$\nabla = \nabla_0 + \epsilon \nabla_1 + \dots. \quad (6)$$

Substituting the expansions (4)–(6) into the original problem (1) and expanding in ϵ , one arrives at a set of equations in different orders of ϵ .

In the lowest order, we reproduce the equation $\mathbf{f}(\nabla_0, \mathbf{u}_0, R) = 0$ determining the basic solution. In the next order, the linear problem (2) is reproduced in the following form:

$$\mathbf{f}_{\mathbf{u}}(\nabla_0) \mathbf{u}_1 = 0, \quad (7)$$

where $\mathbf{f}_{\mathbf{u}} \equiv \partial \mathbf{f} / \partial \mathbf{u}$ and the dependence of $\mathbf{f}_{\mathbf{u}}$ on \mathbf{u}_0 and R_c is not shown explicitly. The solution \mathbf{u}_1 is given by a normal mode (3) with amplitude $a(x_1, t_1, t_2, \dots)$ depending on slower time scales:

$$\mathbf{u}_1 = a\mathbf{U} \exp(ik_c x_0) + a^* \mathbf{U}^* \exp(-ik_c x_0). \quad (8)$$

In the consequent orders, one obtains the equations

$$\mathbf{f}_u(\nabla_0)\mathbf{u}_n = \mathbf{g}_n, \quad (9)$$

where \mathbf{g}_n denotes the n th order inhomogeneity vector. A set of solvability conditions for the normal mode (3) will define slow spatiotemporal dynamics of the amplitude of the mode. It can be shown that only part of the inhomogeneity \mathbf{g}_n , which projects on the principal harmonic of the mode, will contribute into the corresponding solvability condition. Denoting the scalar product by angle brackets and the projection operator on the harmonic $\exp(i\vartheta)$ as $\mathcal{P}[\cdot, \exp(i\vartheta)]$, one can write the solvability condition in the n th order as follows:

$$\langle \mathbf{U}^\dagger, \mathcal{P}(\mathbf{g}_n, e^{ik_c x_0}) \rangle = 0, \quad (10)$$

where \mathbf{U}^\dagger denotes the eigenvector of the adjoint linear problem $\mathcal{L}^\dagger \mathbf{U}^\dagger = 0$.

The linear inhomogeneous problem (9) must be solved with respect to \mathbf{u}_n provided that solvability conditions (10) are satisfied. To this particular solution one must add a homogeneous solution of the corresponding order of smallness. The combined solution is used for the calculations of the next-order inhomogeneity \mathbf{g}_{n+1} .

In the second order in ϵ , we have the inhomogeneous linear problem

$$\begin{aligned} \mathbf{f}_u(\nabla_0)\mathbf{u}_2 = & \partial_1 \mathbf{u}_1 - \frac{1}{2} \mathbf{f}_{uu}(\nabla_0)\mathbf{u}_1 \mathbf{u}_1 \\ & - \mathbf{f}_{uR}(\nabla_0)\mathbf{u}_1 R_1 - \mathbf{f}_{u\nabla}(\nabla_0)\nabla_1 \mathbf{u}_1, \end{aligned} \quad (11)$$

where $\mathbf{f}_{uu} \equiv \frac{\partial^2 \mathbf{f}}{\partial \mathbf{u} \partial \mathbf{u}}$, $\mathbf{f}_{uR} \equiv \frac{\partial^2 \mathbf{f}}{\partial \mathbf{u} \partial R}$, etc. It follows that the condition (10) at this order reads as

$$\mathbf{U}^\dagger \mathbf{U} \partial_1 a - \mathbf{U}^\dagger \mathbf{f}_{uR}(ik_c) \mathbf{U} a R_1 - \mathbf{U}^\dagger \mathbf{f}_{u\nabla}(ik_c) \mathbf{U} \nabla_1 a = 0. \quad (12)$$

Setting $R_1 = 0$ in (12), one obtains the traveling wave solution with constant amplitude written in the comoving coordinate system as

$$\frac{da}{d\zeta_1} = 0, \quad \zeta_1 = x_1 + vt_1, \quad v = \mathbf{U}^\dagger \mathbf{f}_{u\nabla}(ik_c) \mathbf{U} / \mathbf{U}^\dagger \mathbf{U},$$

which implies that the dependence of the amplitude a on the time scale t_1 is given by

$$\partial_1 a = v \nabla_1 a. \quad (13)$$

In order to determine the inhomogeneous solution of the problem

$$\mathbf{f}_u(\nabla_0)\mathbf{u}_2 = \partial_1 \mathbf{u}_1 - \frac{1}{2} \mathbf{f}_{uu}(\nabla_0)\mathbf{u}_1 \mathbf{u}_1 - \mathbf{f}_{u\nabla}(\nabla_0)\nabla_1 \mathbf{u}_1, \quad (14)$$

we note that it can be found as a sum of several components

$$\begin{aligned} \mathbf{u}_2 = & \mathbf{u}_2^{(0)} + \mathbf{u}_2^{(1)} e^{ik_c x} + \mathbf{u}_2^{(-1)} e^{-ik_c x} \\ & + \mathbf{u}_2^{(2)} e^{2ik_c x} + \mathbf{u}_2^{(-2)} e^{-2ik_c x}. \end{aligned} \quad (15)$$

The zero-mode component $\mathbf{u}_2^{(0)}$ satisfies the equation

$$\mathbf{f}_u(0)\mathbf{u}_2^{(0)} = -\mathbf{f}_{uu}(ik_c, -ik_c) \mathbf{U} \mathbf{U}^* |a|^2.$$

The solution of this equation can be written as

$$\mathbf{u}_2^{(0)} = -\mathcal{R}[\mathbf{f}_u(0)] \mathbf{f}_{uu}(ik_c, -ik_c) \mathbf{U} \mathbf{U}^* |a|^2, \quad (16)$$

where $\mathcal{R}[\mathbf{m}]$ denotes the resolvent matrix of the matrix \mathbf{m} ; if the matrix is regular, the resolvent coincides with the

inverse matrix, otherwise, the resolvent is constructed using the spectrum of the original matrix \mathbf{m} . The double-mode component $\mathbf{u}_2^{(2)}$ is found as

$$\mathbf{u}_2^{(2)} = -\frac{1}{2} \mathcal{R}[\mathbf{f}_u(2ik_c)] \mathbf{f}_{uu}(ik_c, ik_c) \mathbf{U} \mathbf{U} a^2. \quad (17)$$

The leading-mode solution $\mathbf{u}_2^{(1)}$ orthogonal to the first-order solution \mathbf{u}_1 reads as

$$\mathbf{u}_2^{(1)} = -\mathcal{R}[\mathbf{f}_u(ik_c)] \mathbf{f}_{u\nabla}(ik_c) \mathbf{U} \nabla_1 a. \quad (18)$$

In the third order in ϵ , we have

$$\begin{aligned} \mathbf{f}_u(\nabla_0)\mathbf{u}_3 = & \partial_2 \mathbf{u}_1 + \partial_1 \mathbf{u}_2 - \frac{1}{6} \mathbf{f}_{uuu}(\nabla_0)\mathbf{u}_1 \mathbf{u}_1 \mathbf{u}_1 - \mathbf{f}_{uu}(\nabla_0)\mathbf{u}_1 \mathbf{u}_2 \\ & - \mathbf{f}_{uR}(\nabla_0)\mathbf{u}_1 R_2 - \mathbf{f}_{uu\nabla}(\nabla_0)\mathbf{u}_1 \nabla_1 \mathbf{u}_1 \\ & - \mathbf{f}_{u\nabla}(\nabla_0)\nabla_1 \mathbf{u}_2 - \frac{1}{2} \mathbf{f}_{u\nabla\nabla}(\nabla_0)\nabla_1^2 \mathbf{u}_1. \end{aligned} \quad (19)$$

The corresponding solvability condition reads as

$$\begin{aligned} & \mathbf{U}^\dagger \mathbf{U} \partial_2 a + \mathbf{U}^\dagger \partial_1 \mathbf{u}_2^{(1)} \\ & = \frac{1}{2} \mathbf{U}^\dagger \mathbf{f}_{uuu}(\nabla_0) \mathbf{U} \mathbf{U} \mathbf{U}^* |a|^2 a + \mathbf{U}^\dagger \mathbf{f}_{uu}(\nabla_0) \mathbf{U} \mathbf{u}_2^{(0)} a \\ & + \mathbf{U}^\dagger \mathbf{f}_{uu}(\nabla_0) \mathbf{U}^* \mathbf{u}_2^{(2)} a^* + \mathbf{U}^\dagger \mathbf{f}_{uR}(\nabla_0) \mathbf{U} a R_2 \\ & + \mathbf{U}^\dagger \mathbf{f}_{u\nabla}(\nabla_0) \nabla_1 \mathbf{u}_2^{(1)} + \frac{1}{2} \mathbf{U}^\dagger \mathbf{f}_{u\nabla\nabla}(\nabla_0) \mathbf{U} \nabla_1^2 a. \end{aligned} \quad (20)$$

The resulting amplitude equation describing the slow dynamics of the perturbation amplitude a can be written in the form

$$\partial_2 a = \alpha a + \kappa |a|^2 a + \delta \nabla_1^2 a, \quad (21)$$

with the linear coefficient proportional to the bifurcation parameter deviation

$$\alpha = \mathbf{U}^\dagger \mathbf{f}_{uR}(ik_c) \mathbf{U} R_2 / (\mathbf{U}^\dagger \mathbf{U}), \quad (22)$$

and the Landau coefficient determining the stability of the perturbation

$$\begin{aligned} \kappa = & (\mathbf{U}^\dagger \mathbf{f}_{uuu}(ik_c, ik_c, -ik_c) \mathbf{U} \mathbf{U} \mathbf{U}^* - 2\mathbf{U}^\dagger \mathbf{f}_{uu}(0, ik_c) \\ & \times \mathbf{U} \{ \mathcal{R}[\mathbf{f}_u(0)] \mathbf{f}_{uu}(ik_c, -ik_c) \mathbf{U} \mathbf{U}^* - \mathbf{U}^\dagger \mathbf{f}_{uu}(2ik_c, -ik_c) \} \\ & \times \mathbf{U}^* \{ \mathcal{R}[\mathbf{f}_u(2ik_c)] \mathbf{f}_{uu}(ik_c, ik_c) \mathbf{U} \mathbf{U} \}) / (2\mathbf{U}^\dagger \mathbf{U}). \end{aligned} \quad (23)$$

The diffusion coefficient δ has the form

$$\begin{aligned} \delta = & \left[\mathbf{U}^\dagger \mathbf{f}_{u\nabla\nabla}(ik_c) \mathbf{U} + 2\mathbf{U}^\dagger \left(\frac{\mathbf{U}^\dagger \mathbf{f}_{u\nabla}(ik_c) \mathbf{U}}{\mathbf{U}^\dagger \mathbf{U}} - \mathbf{f}_{u\nabla}(ik_c) \right) \right. \\ & \left. \times \{ \mathcal{R}[\mathbf{f}_u(ik_c)] \mathbf{f}_{u\nabla}(ik_c) \mathbf{U} \} \right] / (2\mathbf{U}^\dagger \mathbf{U}). \end{aligned} \quad (24)$$

The Ginzburg-Landau equation can be used also in its reduced form (the Landau equation) in the case when the spatial modulation of the perturbation amplitude can be neglected ($\delta = 0$)

$$\partial_2 a = \alpha a + \kappa |a|^2 a. \quad (25)$$

Consider the amplitude dynamics described by the Landau equation (25), the solution of which is given by

$$a(t_2) = a_0 \left(\frac{\alpha}{\alpha + \kappa a_0^2 (1 - e^{2\alpha t_2})} \right)^{1/2}. \quad (26)$$

In steady state, (25) describes a pitchfork bifurcation for the amplitude a of the perturbed solution. The stability of its stationary solution $a_{st} = \sqrt{-\alpha/\kappa}$ is determined by the

sign of the Landau coefficient κ . For positive κ and α , the rupture is inevitable (subcritical bifurcation). For $\alpha > 0$, $\kappa < 0$, the Landau equation (21) may possess stable solutions corresponding to stationary nonruptured corrugated films (supercritical bifurcation). The rupture time t_{rup} estimate can be defined as the time when the original assumption about the smallness of the amplitude a compared to the basic solution is no longer valid. One possible choice of the time rupture estimate is the time when the amplitude reaches some large but finite value $a_0 \ll A < h_0$:

$$t_{\text{rup}} = \frac{1}{2\alpha} \ln \left(1 + \frac{\alpha}{\kappa} (a_0^{-2} - A^{-2}) \right) \approx \frac{1}{2\alpha} \ln \left(1 + \frac{\alpha}{\kappa a_0^2} \right). \quad (27)$$

Noting that the linear coefficient α is proportional to second-order deviation of the bifurcation parameter R_2 , we can find the limiting value of the rupture time at $R_2 \rightarrow 0$:

$$t_{\text{rup}} = \frac{1}{2a_0^2\kappa} \left(1 - \frac{a_0^2}{A^2} \right) \approx \frac{1}{2a_0^2\kappa}, \quad (28)$$

where we have used the fact that $a_0 \ll A$. The estimate (28) indicates that dependence of the rupture time on parameters of the problem is concentrated in the only factor κ^{-1} .

B. Dynamics of the fastest growing mode

Consider the procedure of nonlinear analysis of the problem

$$\partial_t \mathbf{u} = \mathbf{f}(\nabla, \mathbf{u}), \quad (29)$$

assuming that a homogeneous stationary basic n -component state \mathbf{u}_0 is unstable and a single short-wave unstable mode with the fastest growing wave number k_m has the maximum growth rate $\sigma_+ > 0$. We also assume that all other modes are stable with growth rates $\sigma_{-j} < 0$.

The small perturbation $\tilde{\mathbf{u}}_1(x, t)$ of the basic solution in the linear approximation satisfies the equation

$$\partial_t \tilde{\mathbf{u}}_1 = \mathcal{L}(\nabla, \mathbf{u}_0) \tilde{\mathbf{u}}_1, \quad (30)$$

where \mathcal{L} is a linear operator calculated at the point $\mathbf{u} = \mathbf{u}_0$ and $\tilde{\mathbf{u}}_1$ has the form

$$\tilde{\mathbf{u}}_1 = \left(A(t)\mathbf{U} + \sum_{j=2}^n A_j(t)\mathbf{U}_{-j} \right) \exp(ik_m x) + \text{c.c.}, \quad (31)$$

where $A(t)$ and $A_j(t)$ correspond to the amplitude of unstable and j th stable mode, respectively, \mathbf{U}_{-j} is the eigenvector of the linear problem (2) verifying the equation $\mathcal{L}\mathbf{U}_{-j} = \sigma_{-j}\mathbf{U}_{-j}$ and $\mathcal{L}\mathbf{U} = \sigma_+\mathbf{U}$. We assume that the system of eigenvectors $\{\mathbf{U}, \mathbf{U}_{-j}\}$ is the orthonormal one. The value k_m is found from the condition that the growth rate $\sigma_+(k)$ reaches its maximum at $k = k_m$.

For the second harmonics perturbation, we seek in the form

$$\tilde{\mathbf{u}}_2 = \mathbf{u}_2(t) \exp(2ik_m x) + \text{c.c.} \quad (32)$$

The expansion

$$\mathbf{u} = \mathbf{u}_0 + \tilde{\mathbf{u}}_1 + \tilde{\mathbf{u}}_2 + \dots$$

is inserted into the equation (29), and the terms containing harmonics not higher than second are retained. For the first harmonics, we have

$$\begin{aligned} \partial_t A \mathbf{U} + \sum_{j=2}^n \partial_t A_j \mathbf{U}_{-j} \\ = \sigma_+ \mathbf{U} A + \sum_{j=2}^n \sigma_{-j} \mathbf{U}_{-j} A_j + \mathbf{f}_{\mathbf{uu}}(-ik_m, 2ik_m) \mathbf{U}^* \mathbf{u}_2 A^* \\ + \sum_{j=2}^n \mathbf{f}_{\mathbf{uu}}(-ik_m, 2ik_m) \mathbf{U}_{-j}^* \mathbf{u}_2 A_j^* \\ + \frac{1}{2} \mathbf{f}_{\mathbf{uuu}}(ik_m, ik_m, -ik_m) \mathbf{U} \mathbf{U} \mathbf{U}^* |A|^2 A \\ + \frac{1}{2} \sum_{j,k=2}^n \mathbf{f}_{\mathbf{uuu}}(ik_m, ik_m, -ik_m) \mathbf{U}_{-j} \mathbf{U}_{-k} \mathbf{U}^* A_j A_k A^* \\ + \frac{1}{2} \sum_{j,k,l=2}^n \mathbf{f}_{\mathbf{uuu}}(ik_m, ik_m, -ik_m) \mathbf{U}_{-j} \mathbf{U}_{-k} \mathbf{U}_{-l}^* A_j A_k A_l^* \\ + \frac{1}{2} \sum_{j=2}^n \mathbf{f}_{\mathbf{uuu}}(ik_m, ik_m, -ik_m) \mathbf{U} \mathbf{U} \mathbf{U}_{-j}^* A^2 A_j^* \\ + \sum_{j=2}^n \mathbf{f}_{\mathbf{uuu}}(ik_m, ik_m, -ik_m) \mathbf{U} \mathbf{U}^* \mathbf{U}_{-j} |A|^2 A_j \\ + \sum_{j,k=2}^n \mathbf{f}_{\mathbf{uuu}}(ik_m, ik_m, -ik_m) \mathbf{U} \mathbf{U}_{-j} \mathbf{U}_{-k}^* A A_j A_k^*. \end{aligned} \quad (33)$$

The second harmonics equation reads as

$$\begin{aligned} \partial_t \mathbf{u}_2 = \mathbf{f}_{\mathbf{u}}(2ik_m) \mathbf{u}_2 + \frac{1}{2} \mathbf{f}_{\mathbf{uu}}(ik_m, ik_m) \mathbf{U} \mathbf{U} A^2 \\ + \frac{1}{2} \sum_{j,k=2}^n \mathbf{f}_{\mathbf{uu}}(ik_m, ik_m) \mathbf{U}_{-j} \mathbf{U}_{-k} A_j A_k \\ + \sum_{j=2}^n \mathbf{f}_{\mathbf{uu}}(ik_m, ik_m) \mathbf{U} \mathbf{U}_{-j} A A_j. \end{aligned} \quad (34)$$

The solution of (34) in the limit of fast dynamics is found as

$$\begin{aligned} \mathbf{u}_2 = -\frac{1}{2} \mathbf{f}_{\mathbf{u}}^{-1}(2ik_m) \mathbf{f}_{\mathbf{uu}}(ik_m, ik_m) \\ \times \left(\mathbf{U} \mathbf{U} A^2 + \sum_{j,k=2}^n \mathbf{U}_{-j} \mathbf{U}_{-k} A_j A_k + 2 \sum_{j=2}^n \mathbf{U} \mathbf{U}_{-j} A A_j \right). \end{aligned} \quad (35)$$

We introduce a tensor operator \mathbf{P} acting on vectors $\mathbf{a}, \mathbf{b}, \mathbf{c}$,

$$\begin{aligned} \mathbf{P}(\mathbf{a}, \mathbf{b}, \mathbf{c}) = \frac{1}{2} \mathbf{f}_{\mathbf{uuu}}(ik_m, ik_m, -ik_m) \mathbf{a} \mathbf{b} \mathbf{c} - \frac{1}{2} \mathbf{f}_{\mathbf{uu}}(-ik_m, 2ik_m) \\ \times \mathbf{c} \mathbf{f}_{\mathbf{u}}^{-1}(2ik_m) [\mathbf{f}_{\mathbf{uu}}(ik_m, ik_m) \mathbf{a} \mathbf{b}]. \end{aligned} \quad (36)$$

After substitution of the solution (35) into (33), we obtain an equation governing dynamics of all first harmonics

modes:

$$\begin{aligned}
 \partial_t A \mathbf{U} + \sum_{j=2}^n \partial_t A_j \mathbf{U}_{-j} \\
 = \sigma_+ \mathbf{U} A + \sum_{j=2}^n \sigma_{-j} \mathbf{U}_{-j} A_j + \mathbf{P}(\mathbf{U}, \mathbf{U}, \mathbf{U}^*) |A|^2 A \\
 + \sum_{j,k,l=2}^n \mathbf{P}(\mathbf{U}_{-j}, \mathbf{U}_{-k}, \mathbf{U}_{-l}^*) A_j A_k A_l^* \\
 + \sum_{j,k=2}^n \mathbf{P}(\mathbf{U}_{-j}, \mathbf{U}_{-k}, \mathbf{U}^*) A_j A_k A^* \\
 + \sum_{j=2}^n \mathbf{P}(\mathbf{U}, \mathbf{U}, \mathbf{U}_{-j}^*) A^2 A_j^* + 2 \sum_{j=2}^n \mathbf{P}(\mathbf{U}_{-j}, \mathbf{U}, \mathbf{U}^*) |A|^2 A_j \\
 + 2 \sum_{j,k=2}^n \mathbf{P}(\mathbf{U}, \mathbf{U}_{-j}, \mathbf{U}_{-k}^*) A A_j A_k^*. \quad (37)
 \end{aligned}$$

The above equation can be simplified further by dropping the modes with the fastest decay, which are slaved to the dynamics of slower modes. Multiplying (37) from the left by the eigenvector \mathbf{U}^\dagger of the adjoint problem orthogonal to all \mathbf{U}_{-j} , we arrive at the governing equation for the fastest growing mode:

$$\begin{aligned}
 \mathbf{U}^\dagger \mathbf{U} \partial_t A = \sigma_+ \mathbf{U}^\dagger \mathbf{U} A + \mathbf{U}^\dagger \mathbf{P}(\mathbf{U}, \mathbf{U}, \mathbf{U}^*) |A|^2 A \\
 + \sum_{j,k,l=2}^m \mathbf{U}^\dagger \mathbf{P}(\mathbf{U}_{-j}, \mathbf{U}_{-k}, \mathbf{U}_{-l}^*) A_j A_k A_l^* \\
 + \sum_{j,k=2}^m \mathbf{U}^\dagger \mathbf{P}(\mathbf{U}_{-j}, \mathbf{U}_{-k}, \mathbf{U}^*) A_j A_k A^* \\
 + \sum_{j=2}^m \mathbf{U}^\dagger \mathbf{P}(\mathbf{U}, \mathbf{U}, \mathbf{U}_{-j}^*) A^2 A_j^* \\
 + 2 \sum_{j=2}^m \mathbf{U}^\dagger \mathbf{P}(\mathbf{U}_{-j}, \mathbf{U}, \mathbf{U}^*) |A|^2 A_j \\
 + 2 \sum_{j,k=2}^m \mathbf{U}^\dagger \mathbf{P}(\mathbf{U}, \mathbf{U}_{-j}, \mathbf{U}_{-k}^*) A A_j A_k^*, \quad (38)
 \end{aligned}$$

where m denotes a number of retained slow modes. The corresponding equation for the p th decaying mode reads as

$$\begin{aligned}
 \mathbf{U}_{-p}^\dagger \mathbf{U}_{-p} \partial_t A_p = \sigma_{-p} \mathbf{U}_{-p}^\dagger \mathbf{U}_{-p} A_p + \mathbf{U}_{-p}^\dagger \mathbf{P}(\mathbf{U}, \mathbf{U}, \mathbf{U}^*) |A|^2 A \\
 + \sum_{j,k,l=2}^m \mathbf{U}_{-p}^\dagger \mathbf{P}(\mathbf{U}_{-j}, \mathbf{U}_{-k}, \mathbf{U}_{-l}^*) A_j A_k A_l^* \\
 + \sum_{j,k=2}^m \mathbf{U}_{-p}^\dagger \mathbf{P}(\mathbf{U}_{-j}, \mathbf{U}_{-k}, \mathbf{U}^*) A_j A_k A^* \\
 + \sum_{j=2}^m \mathbf{U}_{-p}^\dagger \mathbf{P}(\mathbf{U}, \mathbf{U}, \mathbf{U}_{-j}^*) A^2 A_j^*
 \end{aligned}$$

$$\begin{aligned}
 + 2 \sum_{j=2}^m \mathbf{U}_{-p}^\dagger \mathbf{P}(\mathbf{U}_{-j}, \mathbf{U}, \mathbf{U}^*) |A|^2 A_j \\
 + 2 \sum_{j,k=2}^m \mathbf{U}_{-p}^\dagger \mathbf{P}(\mathbf{U}, \mathbf{U}_{-j}, \mathbf{U}_{-k}^*) A A_j A_k^*. \quad (39)
 \end{aligned}$$

Equations (38) and (39) determine an approximate low-dimensional dynamics of the system.

In the case of a two-component system ($m = 2$), we arrive at the system of two coupled Landau equations ($\mathbf{U}_{-2} \equiv \mathbf{U}_-$)

$$\begin{aligned}
 \mathbf{U}^\dagger \mathbf{U} \partial_t A \\
 = \sigma_+ \mathbf{U}^\dagger \mathbf{U} A + \mathbf{U}^\dagger \mathbf{P}(\mathbf{U}, \mathbf{U}, \mathbf{U}^*) |A|^2 A \\
 + \mathbf{U}^\dagger \mathbf{P}(\mathbf{U}_-, \mathbf{U}_-, \mathbf{U}_-^*) |A_2|^2 A_2 + \mathbf{U}^\dagger \mathbf{P}(\mathbf{U}_-, \mathbf{U}_-, \mathbf{U}^*) A_2^2 A^* \\
 + \mathbf{U}^\dagger \mathbf{P}(\mathbf{U}, \mathbf{U}, \mathbf{U}_-^*) A^2 A_2^* + 2 \mathbf{U}^\dagger \mathbf{P}(\mathbf{U}_-, \mathbf{U}, \mathbf{U}^*) |A|^2 A_2 \\
 + 2 \mathbf{U}^\dagger \mathbf{P}(\mathbf{U}, \mathbf{U}_-, \mathbf{U}_-^*) |A_2|^2 A, \quad (40)
 \end{aligned}$$

$$\begin{aligned}
 \mathbf{U}_-^\dagger \mathbf{U}_- \partial_t A_2 \\
 = \sigma_- \mathbf{U}_-^\dagger \mathbf{U}_- A_2 + \mathbf{U}_-^\dagger \mathbf{P}(\mathbf{U}, \mathbf{U}, \mathbf{U}^*) |A|^2 A \\
 + \mathbf{U}_-^\dagger \mathbf{P}(\mathbf{U}_-, \mathbf{U}_-, \mathbf{U}_-^*) |A_2|^2 A_2 + \mathbf{U}_-^\dagger \mathbf{P}(\mathbf{U}_-, \mathbf{U}_-, \mathbf{U}^*) A_2^2 A^* \\
 + \mathbf{U}_-^\dagger \mathbf{P}(\mathbf{U}, \mathbf{U}, \mathbf{U}_-^*) A^2 A_2^* + 2 \mathbf{U}_-^\dagger \mathbf{P}(\mathbf{U}_-, \mathbf{U}, \mathbf{U}^*) |A|^2 A_2 \\
 + 2 \mathbf{U}_-^\dagger \mathbf{P}(\mathbf{U}, \mathbf{U}_-, \mathbf{U}_-^*) |A_2|^2 A.
 \end{aligned}$$

In a simplest case when all decaying modes may be dropped, (40) reduces to a single equation of the form

$$\partial_t A = \sigma_+ A + \frac{1}{\mathbf{U}^\dagger \mathbf{U}} \mathbf{U}^\dagger \mathbf{P}(\mathbf{U}, \mathbf{U}, \mathbf{U}^*) |A|^2 A. \quad (41)$$

This equation has the form of the Landau equation (25), so the results of the rupture time presented above can be applied in this case too. The Landau coefficient κ reads as

$$\kappa = \mathbf{U}^\dagger \mathbf{P}(\mathbf{U}, \mathbf{U}, \mathbf{U}^*) / (\mathbf{U}^\dagger \mathbf{U}), \quad (42)$$

while the linear coefficient α is just the mode growth rate σ_+ . Thus, the nonlinear rupture time estimate based on the dynamics of the fastest growing mode reads as

$$t_{\text{rup}} = \frac{1}{2\sigma_+} \ln \left(1 + \frac{\sigma_+}{\kappa a_0^2} \right). \quad (43)$$

III. LONG-SCALE EVOLUTION MODELS OF THIN LIQUID FILMS—NEAR-CRITICAL THEORY

The review [5] contains a large number of model equations describing dynamics of thin liquid films valid in *long-scale* approximation for different physical situations. Consider length scales in the x direction defined by the wavelength λ on a film of mean thickness h_* (here and thereafter dimensional quantities are marked with the subscript asterisk). The distortions are considered to be of long scale if $2\pi h_*/\lambda \ll 1$. In this section, we consider some of these models in their most general form, and perform weakly nonlinear analysis for each of them.

A. Thin liquid films on solid surfaces

The evolution of the bounded film of the dimensionless height h scaled with the mean film thickness h_* is governed by a general model

$$h_t = - \left[(\tau + C_x) \left(\frac{h^2}{2} + \beta h \right) \right]_x + \left[\left(\frac{h^3}{3} + \beta h^2 \right) (\mathcal{F} - \Pi)_x \right]_x, \quad (44)$$

with

$$\mathcal{F}(x, t) = \varphi(h) - Ch_{xx}.$$

Here, the x coordinate is nondimensionalized with h_* , time is scaled with h_*/v_* [where v_* denotes the characteristic velocity of the liquid in the x direction (we later use $v_* = \nu/h_*$, where ν is the kinematic viscosity)], τ and Π denote tangential and normal components of the stress scaled with $\mu v_*/h_*$, $C = \sigma/v_*\mu$ is the dimensionless surface tension (*i.e.*, the inverse of a capillary number), $\beta = \beta_*/h_*$ denotes the scaled slip coefficient, and $\varphi = (\partial \Delta G / \partial h)$ is the van der Waals potential made nondimensional with μ/v_*h_* . Restricting ourselves to the case of zero stress $\Pi = \tau = 0$ and constant surface tension $C_x = 0$ reduces (44) to

$$h_t = \left[\left(\frac{h^3}{3} + \beta h^2 \right) \mathcal{F}_x \right]_x. \quad (45)$$

The linear stability analysis of the uniform stationary state $\mathbf{u}_0 = \{h_0\}$ results in a critical value of the wave number corresponding to a stationary bifurcation point $k_c = [-\varphi'(h_0)/C]^{1/2}$. Following a standard procedure, we choose C as a bifurcation parameter. In a bounded domain $0 < x < L$, the basic solution h_0 changes stability with $k = k_c$ and when $C < C_c = -\varphi'(h_0)L^2/4\pi^2$, where C_c correspond to a steady bifurcation point.

To investigate the weakly nonlinear problem in the vicinity of the bifurcation point, we expand the bifurcation parameter as $C = C_c + \epsilon^2 C_2 + \dots$, where ϵ is a small criticality, we introduce a slow time scale suggested by the linear theory $t_2 = \epsilon^2 t$, and we seek the solution in power series of ϵ as $h = h_0 + \epsilon h_1 + \dots$. Substitution of this expansion into (45) to the first order in ϵ yields $h_1 = a(t_2)e^{ik_c x} + c.c.$. The perturbation amplitude a satisfies the dynamic Landau equation (25) derived using the near-critical perturbation theory of Sec. II with the coefficients given by (22) and (23):

$$\begin{aligned} \alpha &= -6\xi\varphi^2(h_0)\frac{C_2}{C_c}, \\ \kappa &= \xi[\varphi''(h_0) + 3\varphi'(h_0)\varphi'''(h_0)], \\ \xi &= \frac{(1 + 3B)h_0^3}{18C_c}, \end{aligned} \quad (46)$$

where $B = \beta/h_0$. Comparison of (46) with the general formulas for the Landau equation implies that the perturbation saturates only if the following inequalities hold:

$$\varphi'(h_0) < 0, \quad \varphi''(h_0)^2 + 3\varphi'(h_0)\varphi'''(h_0) < 0, \quad (47)$$

where the first inequality represents a condition of bifurcation existence ($k_c^2 = -\varphi'/C_c > 0$). Several typical potentials used in thin-film models are mentioned in [5]. It can be readily seen

that the conditions (47) can be satisfied only if the potential $\varphi(h_0)$ is a sum of *antagonistic* (attractive and repulsive) interactions. Since $\xi > 0$, it is readily seen from (46) that, for purely attractive potential, κ is always positive and the rupture is inevitable.

When the antagonistic attractive and repulsive intermolecular interactions are present, nonlinear saturation of the rupture instability is possible as κ may change sign (supercritical bifurcation). Let us consider the most popular representation of the antagonistic van der Waals potential for unstructured thin films [11, 12] (for example, simple liquids and amorphous polymers)

$$\varphi(h) = \frac{\mathcal{A}}{h^c} - \frac{\mathcal{B}}{h^d} - (S_p/l_p)e^{-h/l_p}, \quad (48)$$

where $\mathcal{A} = \mathcal{A}_*/6\pi\rho v^2 h_*^{c-2}$ denotes the effective Hamaker constant for the van der Waals interaction with a semi-infinite thick substrate (for example, silicon), and its positive and negative values denote long-range attraction and repulsion, respectively; $S_p = S_{p*}h_*^2/\rho v^2$ is the dimensionless strength of the medium-range attraction ($S_p < 0$) or repulsion ($S_p > 0$) with $l_p = l_{p*}/h_*$ being its scaled correlation (decay) length; and $\mathcal{B} = \mathcal{B}_*/\rho v^2 h_*^{d-2}$ is the scaled constant of the effective short-range contact repulsion ($\mathcal{B} > 0$). For the potential (48), the condition (47) translates to

$$d\gamma_1 + H\gamma_2 < c, \quad \sum_{i,j} \sum_{i+j \leq 2} a_{ij}\gamma_1^i \gamma_2^j < 0, \quad (49)$$

where the first inequality is imposed by the linear theory, $\gamma_1 = \mathcal{B}h_0^{c-d}/\mathcal{A}$, $\gamma_2 = (S_p/l_p)h_0^c e^{-H}/\mathcal{A}$, $H = h_0/l_p$, and a_{ij} are some polynomial functions of c, d , and H only.

When the interplay between algebraic potentials is considered ($\gamma_2 = 0$), the nonlinear stability region is defined by γ_1 alone. For the exponents $(c, d) = (3, 4)$ (repulsive retarded van der Waals potential, e.g., [16]), the film does not exhibit nonlinear rupture for $0.51 \lesssim \gamma_1 \lesssim 0.73$, while from the first inequality in (49), the film is linearly unstable for $\gamma_1 < \frac{3}{4}$.

For the exponents $(c, d) = (3, 9)$ (short-range Born repulsion), the stability window is shifted to lower values of γ_1 and the film is stable whenever $0.066 < \gamma_1 < 0.30$ (the film is linearly unstable for $\gamma_1 < \frac{1}{3}$). For instance, using the values of the Hamaker constants measured for a polystyrene film on oxidized Si wafers (type-C wafers in [15]: PS film on Si/SiO wafers with an oxide layer thickness of ~ 191 nm) with $\mathcal{A}_* = 2.2 \times 10^{-20}$ J and $\mathcal{B}_* = 5.04 \times 10^{-75}$ J m⁶ [14], the nonlinear analysis via the second inequality in (49) predicts a nonruptured film thickness of $h_* \approx 2$ nm ($\gamma_1 = 0.068$), while the linear theory via the first inequality in (49) anticipates the critical thickness of $h_* \approx 1.53$ nm and the equilibrium thickness determined from the minimum of ΔG is only 1.3 nm [14]. For thicker films, γ_1 is rapidly decreasing as h_*^{-6} , e.g., $\gamma_1 \approx 0.00125$ for $h_* = 3.9$ nm.

When the interplay between algebraic and exponential potentials is concerned ($\gamma_1 = 0$), the nonlinear stability diagram can be defined in terms of γ_2 and H as in Fig. 1(a). The dashed lines correspond to the boundary of linear stability, while the regions of nonlinear saturation (supercritical bifurcation) corresponding to $\kappa < 0$ in (46) are shown in gray (regions iii and iv). Note that, if the long-range attraction is combined with the shorter-range repulsion ($\mathcal{A} > 0$, $S_p > 0$), the spinodally

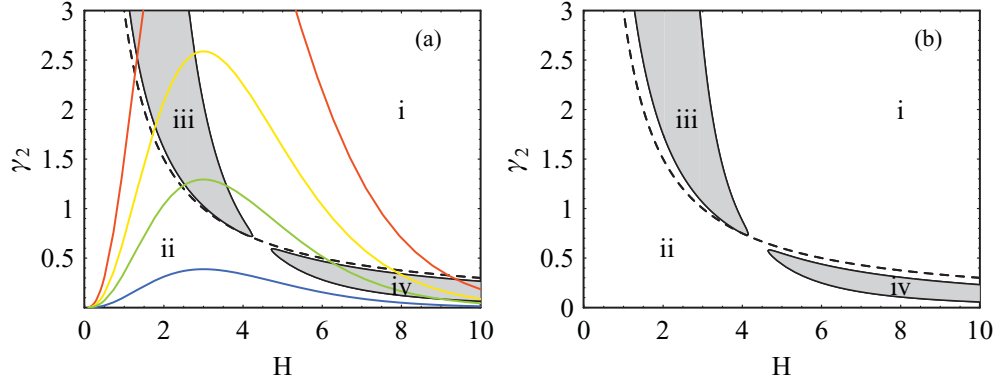


FIG. 1. (Color online) Stability diagram for an antagonistic exponential (algebraic) potential ($\gamma_1 = 0$) in plane of parameters $\gamma_2 = (S_p/l_p)h_0^c e^{-h_0/l_p}/\mathcal{A}$ and $H = h_0/l_p$. The dashed curves correspond to marginal stability boundary for $c = 3$. Colored solid curves on (a) show the dependence of γ_2 on H upon varying hydrophobicity of the substrate from hydrophilic (blue, lower curve) to hydrophobic (red, upper curve) using parameters from Ref. [12]. The regions of supercritical stabilization ($\kappa < 0$) are shown in gray: (a) near-critical theory, $\zeta = 1$ ($k = k_c$); (b) fastest growing mode, $\zeta = 1/2$ ($k = k_m$).

unstable region is below the dashed curve (region ii in Fig. 1), and nonlinear saturation occurs for $H \gtrsim 4.5$ and small values of γ_2 (region iv). In the opposite case ($\mathcal{A} < 0$, $S_p < 0$), the spinodally unstable region lies above the dashed curve (region i) and nonlinear saturation takes place for thinner films $H \lesssim 4$, and moderate values of γ_2 (region iii). For instance, for aqueous films on Si substrates with $c = 3$, $\mathcal{A}_* = -1.41 \times 10^{-20}$ J, and $l_{p*} = 0.6$ nm [12], we plot γ_2 versus H in Fig. 1 (color solid curves) for different values of S_{p*} varying from -0.61 mJ/m² (blue, lower curve) to -8.5 mJ/m² (red, upper curve) due to increasing hydrophobicity of the substrate [12]. It is evident from Fig. 1(a) that the emergence of nonruptured ultrathin films is possible on nonhydrophilic substrates as the color curves cross region (iii), while on hydrophilic substrates (the blue curve), the film of any thickness is stable, in accord with [12].

Even more interesting is the behavior for competing short-range algebraic and exponential potentials. In this case, $\gamma_1, \gamma_2 \neq 0$ and as they both vary with h_0 , we chose to depict the stability diagram in terms of dimensional quantities S_{p*} and h_* as in Fig. 2. It is evident that stabilization is possible for a wide range of film thicknesses h_* . When the magnitude of the exponential repulsion is small, the steady nonruptured state is only possible for ultrathin films; for moderate values of S_{p*} , the band of stable solutions widens. For instance, when $S_{p*} = 1.1$ mJ/m², with parameters corresponding to the red curve in Fig. 5, nonlinear theory predicts that the film is stable below a thickness of ~ 4 nm, whereas linear stability provides a value of ~ 2.2 nm.

Finally, we consider van der Waals interactions of the polystyrene films with SiO coating on Si substrate (in dimensional form)

$$\varphi_* = \frac{\mathcal{A}_{*Si} - \mathcal{A}_{*SiO}}{6\pi(h_* + d_*)^3} + \frac{\mathcal{A}_{*SiO}}{6\pi h_*^3} - \frac{\mathcal{B}_*}{h_*^9}, \quad (50)$$

with $\mathcal{A}_{*Si} = -1.3 \times 10^{-19}$ J, $\mathcal{A}_{*SiO} = 2.2 \times 10^{-20}$ J, and $\mathcal{B}_* = 5.04 \times 10^{-75}$ J m⁶ [15]. In this case, the stability diagram can be depicted in terms of the film thickness h_* and the SiO coating thickness d_* in Fig 3(a). Again, there is a narrow stability window for ultrathin films up to ~ 2 nm, while its

width is insensitive to the variation in SiO coating thickness. The stabilization for thicker films does not materialize similar to the previously discussed case of exponents $(c, d) = (3, 9)$ without coating. The plot of the rupture time estimate in Fig. 3(b) for C-type wafers in [15] with the thick SiO coating $d_* = 191$ nm shows that the rupture time is fast increasing with the increase in the film thickness as $(\partial\varphi/\partial h) \rightarrow 0$, and that it diverges near $h_* \approx 2$ nm at the boundary of the nonlinear stabilization.

The existence of the region corresponding to the nonruptured states next to the spinodal boundary $(\partial\varphi/\partial h) = 0$ is in accord with the general findings regarding the transition between the dewetting dynamics deep inside the spinodal territory, where the prediction of linear theory for the length and time scales of instability agrees with the results of numerical simulations, and close to the critical thickness where $(\partial\varphi/\partial h) \rightarrow 0$, where the correlation with the linear scales is lost [11]. The legitimate question is whether the near-critical

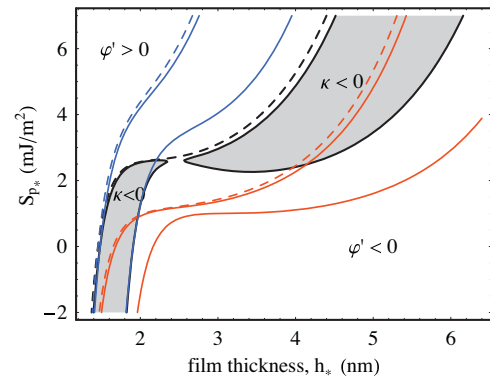


FIG. 2. (Color online) Stability diagram for a general van der Waals potential (48). The regions to the right to the dashed curves are linearly unstable and the regions between the solid curves correspond to the stationary nonruptured state. Black curves correspond to $\mathcal{A}_* = 3.0 \times 10^{-20}$ J, $\mathcal{B}_* = 5.04 \times 10^{-75}$ J m⁶, and $l_{p*} = 0.6$ nm (regions of supercritical stability are shown in gray). The color curves correspond to the same values of the parameters except $l_{p*} = 0.4$ nm (blue, upper curves) and $\mathcal{A} = 1.4 \times 10^{-20}$ J (red, lower curves).

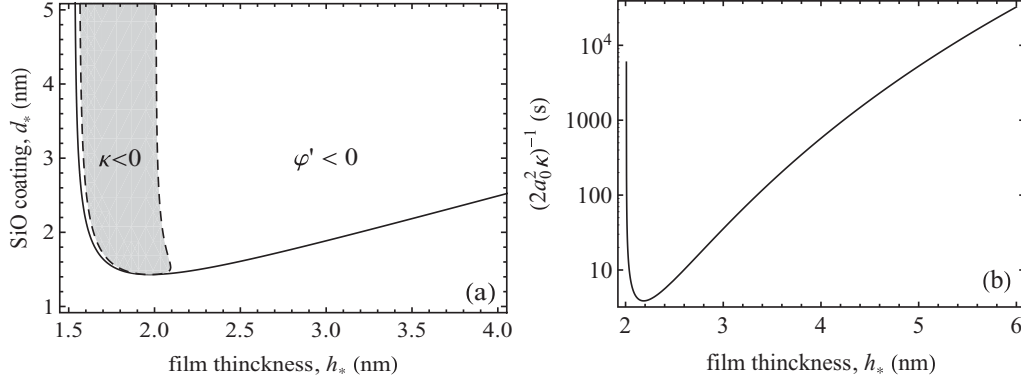


FIG. 3. Stability of a thin film on coated solid substrate for a potential (50) for the parameters $\mathcal{A}_{*Si} = -1.3 \times 10^{-19}$ J, $\mathcal{A}_{*SiO} = 2.2 \times 10^{-20}$ J, and $\mathcal{B}_* = 5.04 \times 10^{-75}$ J m⁶ corresponding to air/PS/SiO in [15]. (a) The stability map in terms of the film thickness h_* and the coating thickness d_* . The region above the solid curve corresponds to the linearly unstable state with $\varphi'(h) < 0$. The dashed curve marks the boundary of supercritical bifurcation corresponding to a stable nonruptured state $\kappa < 0$. (b) The near-critical rupture time estimate $\sim (2a_0^2\kappa)^{-1}$ vs the film thickness h_* for type-C wafers with $d_* = 191$ nm and the initial perturbation amplitude $a_0 = 0.1$ nm.

theory that is formally valid for perturbation with a wave number k_c is applicable for an arbitrary wavelength k . In fact, in the experiments or simulations, the disturbances with the wavelengths $k < k_c$ are admissible and far from the instability threshold (deep inside spinodal territory) and the lengthscale is dictated by the fastest growing mode at $k = k_m$. We address this issue in Sec. IV in detail where we compare the near-critical analysis with a more general (though less rigorous) analysis of instability at arbitrary wavelength.

B. Film on solid surface: Strong slippage

In [20], the different model equations describing the dynamics of thin liquid films on solid substrates were derived under scaling arguments corresponding to various slippage regimes (weak, moderate, and strong). In this case, the use of the standard lubrication approximation is not valid and the derivation is analogous to that in [7], which yields two coupled evolution equations for the film thickness h and the tangential velocity u :

$$\begin{aligned} h_t &= -(uh)_x, \\ hu_t &= -huu_x - h\mathcal{F}_x - \frac{u}{\beta} + (4hu_x)_x. \end{aligned} \quad (51)$$

It can be readily seen that these model equations for an infinite slippage $\beta \gg 1$ become identical to the equations describing dynamics of free films (53) with no surfactant ($\Gamma = 0$). The amplitude equation (25) coefficients for this model read as

$$\begin{aligned} \alpha &= -6\xi\varphi'^2(h_0)\frac{\mathcal{C}_2}{\mathcal{C}_c}, \\ \kappa &= \xi[\varphi''^2(h_0) + 3\varphi'(h_0)\varphi'''(h_0)], \\ \xi &= \frac{h_0^3 B}{6[\mathcal{C}_c + 4h_0^2 B\varphi'(h_0)]}, \end{aligned} \quad (52)$$

where $B = \beta/h_0$. Note that, for $\xi > 0$, the stability conditions (47) remain unchanged.

C. Free film with insoluble surfactant

The dynamics of the *free* film with insoluble surfactants was considered in [7,9]. The governing set of equations for the

film thickness h scaled with the mean thickness h_* , tangential velocity u scaled with v/h_* , and surfactant concentration Γ scaled with some typical equilibrium value Γ_* has the form

$$\begin{aligned} h_t &= -(uh)_x, \\ \Gamma_t &= \frac{\Gamma_{xx}}{\mathcal{P}} - (\Gamma u)_x, \\ hu_t &= -huu_x - h\mathcal{F}_x + (4hu_x - \mathcal{M}\Gamma)_x, \end{aligned} \quad (53)$$

where as before $\mathcal{F} = \varphi(h) - \mathcal{C}h_{xx}$. Here φ is the van der Waals potential nondimensionalized with $\rho v^2/h_*^2$, $\mathcal{C} = \sigma_* h_*/\rho v^2$ is the dimensionless surface tension for the constant part of the tension σ_* at concentration Γ_* , $\mathcal{P} = v/D_s$ is the Péclet number, where D_s is the surface diffusivity, and $\mathcal{M} = (-\partial\sigma/\partial\Gamma)\Gamma_* h_*/\rho v^2$ is the Marangoni number. The basic solution of (53) corresponds to the film of constant thickness h_0 with homogeneous surfactant concentration Γ_0 and zero tangential velocity.

For this problem, we obtain the simple expression for the coefficients

$$\begin{aligned} \alpha &= -6\xi\varphi'^2(h_0)\frac{\mathcal{C}_2}{\mathcal{C}_c}, \\ \kappa &= \xi[\varphi''^2(h_0) + 3\varphi'(h_0)\varphi'''(h_0)], \\ \xi &= \frac{h_0^2}{6[\lambda\mathcal{C}_c + 4h_0\varphi'(h_0)]}, \end{aligned} \quad (54)$$

where $\lambda = \mathcal{M}\mathcal{P}\Gamma_0$. As before, for $\xi > 0$, the stability conditions (47) remain unchanged.

D. Weakly slipping film with insoluble surfactant

The long-scale approximation model for the weakly slipping films with insoluble surfactant on solid substrate derived in [10] can be written in compact form using the same nondimensionalization as before [19]:

$$\begin{aligned} h_t &= \left[\mathcal{M}\Gamma_x h \left(\frac{h}{2} + \beta \right) + \mathcal{F}_x h^2 \left(\frac{h}{3} + \beta \right) \right]_x, \\ \Gamma_t &= \frac{\Gamma_{xx}}{\mathcal{P}} + \left[\mathcal{M}\Gamma\Gamma_x (h + \beta) + \Gamma\mathcal{F}_x h \left(\frac{h}{2} + \beta \right) \right]_x. \end{aligned} \quad (55)$$

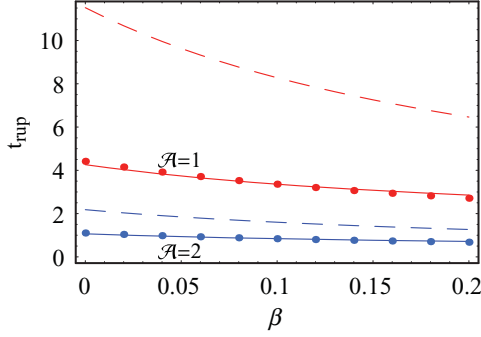


FIG. 4. (Color online) Variation of the rupture time t_{rup} with β for $h_0 = 1$, $C = 1$, $\mathcal{M} = 1$, $\mathcal{P} = 100$, $\Gamma_0 = 0.5$, $c = 3$, and $\mathcal{A} = 1$ (red), $\mathcal{A} = 2$ (blue). The solid curves correspond to the near-critical theory [Eqs. (28) and (56)] with $a_0 = 0.108$, the dots correspond to the results of numerical simulations of [10], and the dashed curves are the prediction of the linear stability.

The linear coefficient α and the Landau coefficient κ in this case are given by

$$\alpha = -6\xi\varphi'^2(h_0)\frac{C_2}{C_c}, \quad (56)$$

$$\kappa = \xi[\varphi''^2(h_0) + 3\varphi'(h_0)\varphi'''(h_0)],$$

respectively, and

$$\xi = \frac{h_0^3 [4(1 + 3B) + \lambda h_0(1 + 4B)]}{72C_c [1 + \lambda h_0(1 + B)]},$$

$$\lambda = \mathcal{M}\mathcal{P}\Gamma_0, \quad B = \beta/h_0.$$

For the most commonly encountered attractive potential $\varphi = \mathcal{A}/h^c$ with $c = 3$, we calculate the rupture time from (28), where κ is given by (56), and compare the result with findings of the numerical simulations of the original evolution equations (55) reported by [10]. Here again $\mathcal{A} = \mathcal{A}_*/6\pi\rho v^2 h_*^{c-2} > 0$ is the scaled attractive Hamaker constant with h_* being the mean film thickness.

Figure 4 shows the dependence of the rupture time t_{rup} on slippage length β (solid lines) versus the simulation results [10] (the dots) for two distinct values of the scaled Hamaker constant \mathcal{A} . It is readily seen that there is a very close agreement between the theoretical prediction and simulation results. Since the numerical simulations refer to the fastest growing mode, the amplitude of the initial perturbation used here ($a_0 = 0.108$) is different from that used in [10] ($a_0 = 0.01$) and is chosen to best fit numerical results. Nevertheless, a very close agreement between the results of the near-critical theory and the numerical simulations upon varying \mathcal{A} and β suggests that the near-critical theory can be adequately applied to model rupture even far from the instability threshold. Note that the prediction of the linear stability theory is rather poor in this case (dashed lines) as it overestimates the rupture time by $\sim 100\%$.

In Fig. 5, the same dependence of t_{rup} on β as in Fig. 4 is depicted (in linear-log coordinates) except now we vary \mathcal{M} while keeping the amplitude of the initial disturbance fixed at $a_0 = 0.108$. There is a very close agreement between the theoretical prediction and the numerical results [10], with both showing a weak impact of the Marangoni stresses on rupture

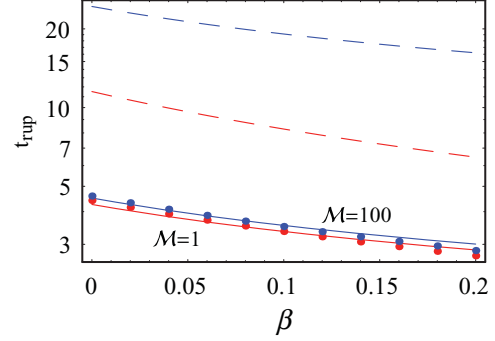


FIG. 5. (Color online) Variation of the rupture time t_{rup} with β (linear-log plot) for $\mathcal{A} = 1$ and the same values of other parameters as in Fig. 4 except we vary \mathcal{M} : $\mathcal{M} = 1$ (red), $\mathcal{M} = 100$ (blue). The solid curves correspond to the near-critical theory [Eqs. (28) and (56)] with $a_0 = 0.108$, the dots correspond to the results of numerical simulations of [10], and the dashed curves are the prediction of the linear stability.

time. On the other hand, the linear estimate anticipates that the increase in \mathcal{M} may appreciably stabilize the film against rupture. Such stabilization is expected since any deformation of the film is associated with the liquid flow out of the thinner regions into the thicker regions due to continuity. The surfactant is redistributed by the flow in a way that its concentration is higher at the elevated portions of the film. The resulting gradients of the surface tension (lower surface tension at the elevated portions and higher surface tension at the depressions) will drive the liquid flow toward the regions of higher surface tension opposing the flow yielding the initial deformation and thus stabilizing the film. This stabilization is also evident upon examining the dispersion relation of linear stability analysis: the maximum growth rate σ_m decreases with the increase in \mathcal{M} [10]. However, for $\mathcal{M} = 100$, the deviation between the linear and the nonlinear estimate is $\sim 400\%$, which shows unequivocally that application of linear stability may yield quite inaccurate estimates of the film rupture time.

In Fig. 6, we present the variation of the rupture time upon varying the surface tension C . Again, the rupture time estimate

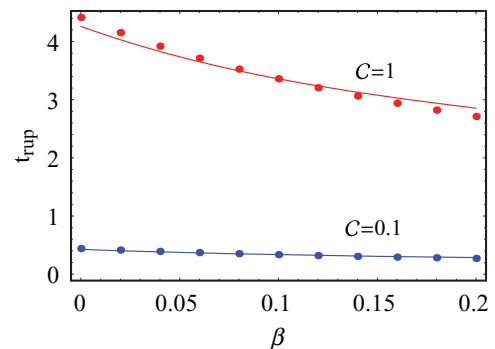


FIG. 6. (Color online) Variation of rupture time with β for $\mathcal{A} = 1$ and the same values of other parameters as in Fig. 4 except we vary C : $C = 1$ (red), $C = 0.1$ (blue). The solid curves correspond to the near-critical theory [Eqs. (28) and (56)] for $a_0 = 0.108$ and the dots correspond to the results of numerical simulations [10].

based on weakly nonlinear theory, computed for the same fixed amplitude of the initial disturbance $a_0 = 0.108$, is in excellent agreement with the results of numerical simulations [10]. It is evident that lowering surface tension destabilizes the film, while the effect of the slippage is more pronounced for higher \mathcal{C} .

Note the use of the same value of the amplitude of initial perturbation $a_0 = 0.01$ as in the numerical simulation in [10] instead of $a_0 = 0.108$, and the weakly nonlinear rupture time estimate (28) would result in a simple shift of solid curves in Figs. 4, 5, and 6 upward by a factor of ~ 100 since $t_{\text{rup}} \sim 1/a_0^2$.

IV. LONG-SCALE EVOLUTION MODELS OF THIN LIQUID FILMS—FASTEST GROWING MODE

A. Thin liquid films on solid substrate

Let us show how the general analysis of the weakly nonlinear dynamics far from the instability threshold of Sec. II B can be applied for derivation of rupture time estimates without any adjustable parameters.

First, consider the dynamics of the thin liquid film on the solid substrate described by the evolution equation (45). In this case, the wave number k_m corresponding to the fastest growing mode satisfies the relation $2\mathcal{C}k_m^2 + \varphi'(h_0) = 0$, and the growth rate σ_+ reads as

$$\sigma_+ = \frac{h_0^3(1+3B)}{12\mathcal{C}}\varphi'^2(h_0) = \frac{h_0^3(1+3B)\mathcal{C}}{3}k_m^4, \quad (57)$$

where as before $B = \beta/h_0$. The computation of the Landau coefficient applying the general formula (42) yields the simple closed-form result

$$\kappa = \frac{h_0^3(1+3B)}{12\mathcal{C}}[\varphi'^2(h_0)]'' - \frac{h_0(11+44B+48B^2)}{16\mathcal{C}(1+3B)}\varphi'^2(h_0). \quad (58)$$

Note that the closed-form expression for κ in (58) no longer has the same structure as that in the near-critical case (46).

Nevertheless, one may pose a problem of derivation of the Landau equation using the Galerkin method for an arbitrary value of the wave number k . Setting

$$k^2 = -\zeta\varphi'(h_0)/\mathcal{C}, \quad 0 \leq \zeta \leq 1, \quad \varphi'(h_0) < 0,$$

the growth rate is obtained as

$$\begin{aligned} \sigma_+ &= \frac{h_0^3(1+3B)}{3\mathcal{C}}\zeta(1-\zeta)\varphi'^2(h_0) \\ &= \frac{h_0^3(1+3B)(1-\zeta)\mathcal{C}}{3\zeta}k^4, \end{aligned} \quad (59)$$

and the Landau coefficient has the form

$$\begin{aligned} \kappa &= \frac{\zeta h_0^3(1+3B)}{6\mathcal{C}(4\zeta-1)}[\varphi''^2(h_0) + (4\zeta-1)\varphi'''(h_0)\varphi'(h_0)] \\ &\quad - \frac{\zeta(1-\zeta)h_0}{2\mathcal{C}(4\zeta-1)(1+3B)}[(13\zeta-1)(1+4B) \\ &\quad + 6(10\zeta-1)B^2]\varphi'^2(h_0). \end{aligned} \quad (60)$$

The above formulas reduce to (58) at $\zeta = \frac{1}{2}$ and to (46) at $\zeta = 1$ corresponding to the fastest growing mode, the wave number k_m , and the near-critical mode $k = k_c$, respectively. The growth

rate is non-negative, and this means that negative values of the Landau coefficient (60) correspond to the saturated state, which may further coarsen to produce the nonruptured film. It is interesting that κ changes sign at $\zeta = \frac{1}{4}$, which corresponds to the long-wavelength perturbations with $k < k_m$.

For the most common form of attractive van der Waals potential (48) (with only nonzero \mathcal{A} and $c = 3$), one finds for $\zeta = \frac{1}{2}$ the explicit expressions

$$\begin{aligned} \kappa_c &= 38\mu, \quad \sigma_+ = 3\mu h_0^2/4, \\ \kappa_m &= 9\mu \left(3 - \frac{11+44B+48B^2}{16(1+3B)^2} \right), \\ \mu &= \frac{\mathcal{A}^2(1+3B)}{\mathcal{C}h_0^7}. \end{aligned}$$

Here κ_c, κ_m denote the Landau coefficients for k_c, k_m , respectively. All three quantities ($\sigma_+, \kappa_c, \kappa_m$) determining the rupture time values scale with the same parameter μ . It can be verified by straightforward computation that the term in the brackets in the expression for κ_m does not vary significantly in the characteristic interval of values $0 \leq \beta \leq 0.2$ of the slip coefficient and thus $\kappa_m \approx 20\mu$. In this approximation, the rupture time given by (43) is similar to that given by (28), the only difference being the logarithmic factor that depends only on the value of a_{0m} selected for the fastest growing mode. Therefore, fitting the value of a_{0c} for the critical mode in (28), one can always reproduce the proper quantitative dependence of the rupture time on governing parameters of the problem at fastest growing mode with k_m . The corresponding value of a_{0c} is found from the following condition for the prescribed value of the initial disturbance a_{0m} :

$$\frac{1}{76a_{0c}^2} \approx \frac{2}{3h_0^2} \ln \left(1 + \frac{h_0^2}{20a_{0m}^2} \right). \quad (61)$$

Let us now consider the general representation of the antagonistic van der Waals potential (48). It can be shown that stability of disturbance with an arbitrary wavelength with $0 \leq \zeta \leq 1$ ($0 \leq k \leq k_c$) is governed by the inequality of the same form as (49):

$$\sum_{i,j} \sum_{i+j \leq 2} a_{ij} \gamma_1^i \gamma_2^j < 0, \quad (62)$$

where a_{ij} are now some polynomial functions of c, d, H , and ζ .

When the interplay between algebraic potentials is considered ($\gamma_2 = 0$), the nonlinear stability region is defined by γ_1 alone. For exponents $(c, d) = (3, 4)$ (repulsive retarded van der Waals force), the film is stable if $0.50 < \gamma_1 < 0.70$. This estimate is very close to the analogous result obtained from near-critical theory $0.51 < \gamma_1 < 0.73$. For the exponents (3) and (9) (short-range Born repulsion), the nonlinear rupture at k_m is suppressed for $0.059 < \gamma_1 < 0.25$, while the near-critical theory gave a very close estimate $0.066 < \gamma_1 < 0.30$.

When a more general antagonistic attractive and repulsive intermolecular potential (48) is considered, the location of the nonlinear saturation region based on the stability of fastest growing mode at k_m in the corresponding parameter space is very close to the prediction of the near-critical theory. For example, for the antagonistic exponential and algebraic

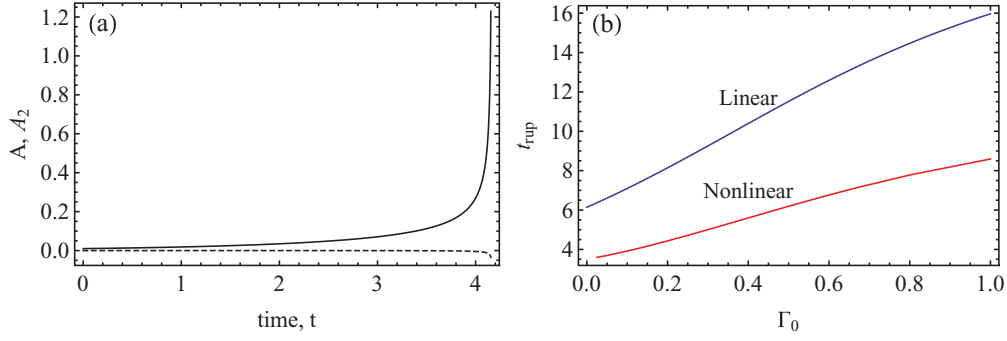


FIG. 7. (Color online) Rupture time estimate from numerical integration of Eqs. (63) and (64) for $\mathcal{A} = 1$, $\beta = 0$, and the same values of other parameters (except Γ_0) as in Fig. 4. (a) Amplitude dynamics for $\Gamma_0 = 0.15$ and the initial values of A (solid) and A_2 (dashed) corresponding to $\{\tilde{h}(0), \tilde{\Gamma}(0)\} = \{0.01, 0\}$. (b) The computed dependence of the rupture time on Γ_0 (red, lower curve) in comparison with the analogous linear estimate (blue, upper curve).

potential ($\gamma_1 = 0$), the location of the nonlinear stability boundary depicted in the plane of parameters γ_2 and H in Fig. 1(b) is quite close to that in Fig. 1(a), where the analogous result of the near-critical theory is provided. The location of the boundary of supercritical bifurcation corresponding to $\kappa = 0$, where κ is provided by Eq. (58), for a general van der Waals potential (48) and for thin film on coated solid substrate for a potential (50) is almost indistinguishable from those in Figs. 2 and 3, respectively, determined using near-critical theory.

B. Weakly slipping film with insoluble surfactant

For a two-component system describing the dynamics of weakly slipping film (55) investigated numerically in [10], two coupled Landau equations (40) are required. In this case, no simple closed-form result is available, and even the linear stability analysis requires numerical solution of the equation $\partial\sigma/\partial k = 0$, where $\sigma(k)$ is the dispersion relation. The coefficients are computed for the given set of parameters at the fastest growing wave number $k = k_m$ and the resulting amplitude equations are solved numerically using the Mathematica built-in ODE integrator NDSolve. For example,

for $\mathcal{A} = 1$, $\beta = 0$, $\Gamma_0 = 0.15$, and the same set of parameters as in Fig. 1, we obtain the following system of coupled amplitude equations:

$$\begin{aligned} \partial_t A &= 0.61A + 40.66A^3 - 3.82A_2^3 \\ &\quad + 56.87A_2^2A + 133.30A_2A^2, \end{aligned} \quad (63)$$

$$\begin{aligned} \partial_t A_2 &= -0.08A_2 + 0.96A_2^3 - 0.10A_2^2A \\ &\quad - 10.82A_2A^2 - 1.50A^3. \end{aligned} \quad (64)$$

Numerical integration of (63) and (64) yields a finite blowup time that is considered as the nonlinear rupture time $t_{\text{rup}} \approx 4.16$. The evolution of the two amplitudes is depicted in Fig. 7(a). The dependence of the computed rupture time as a function of the initial surfactant concentration Γ_0 is shown together with the analogous linear stability estimate $t_{\text{rup}} \sim -\sigma_m^{-1} \ln \frac{\tilde{h}}{h_0}$, as depicted in Fig. 7(b). It is readily seen that the two estimates can differ by a factor of ~ 2 .

Lastly, we compare the results of the nonlinear estimate at the fastest growing mode k_m with the results of numerical calculations in [10]. Figure 8 shows the dependence of the rupture time t_{rup} on slippage length β (solid lines) versus the simulation results [10] (dots) for two distinct values of the scaled Hamaker constant $\mathcal{A} = 1, 2$ for the same set of other parameters as in Fig. 4, where the analogous prediction based on near-critical theory is provided. The initial amplitude of the disturbance is the same as in numerical simulation $\{\tilde{h}(0), \tilde{\Gamma}(0)\} = \{0.01, 0\}$, and there are no adjustable parameters involved. It is readily seen that the agreement between the theory and the numerical integration of the original evolution equations [10] is very good. The dashed lines correspond to the prediction of the reduced model with constant surface tension (43) with (58), with the initial amplitude $a_0 = 0.01$ as in the numerical solution by [10].

In Fig. 9, we show the analogous comparison upon varying the scaled surface tension \mathcal{C} . Again, the rupture time estimate based on the nonlinear theory at k_m (solid lines), computed for the same amplitude of the initial disturbance as in Fig. 8, is in excellent agreement with the results of numerical simulations [10] (dots). The prediction of the reduced model (dashed lines) is also in accord with the results of numerical integrations of the evolution equations.

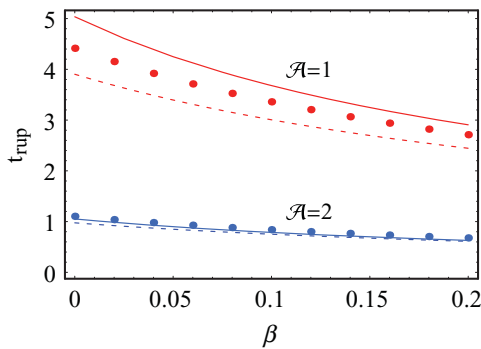


FIG. 8. (Color online) Variation of rupture time vs β with $h_0 = 1$, $\mathcal{C} = 1$, $\mathcal{M} = 1$, $\mathcal{P} = 100$, $\Gamma_0 = 0.5$, $c = 3$, and $\mathcal{A} = 1$ (red), $\mathcal{A} = 2$ (blue). The solid curves correspond to the nonlinear dynamics at k_m (40) with the initial perturbation $\{\tilde{h}(0), \tilde{\Gamma}(0)\} = \{0.01, 0\}$, the dashed lines correspond to the reduced model with constant surface tension (43) with (58) and $a_0 = 0.01$, and the dots correspond to the results of numerical simulations of the original evolution equations [10].

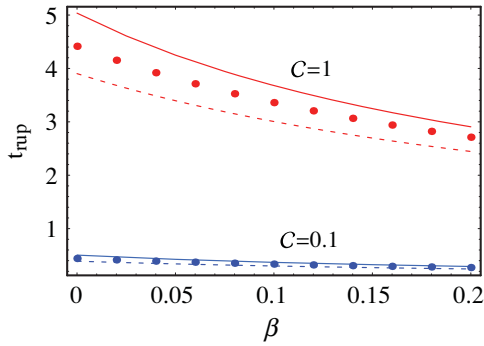


FIG. 9. (Color online) Rupture time vs β for $\mathcal{A} = 1$ and the same values of other parameters as in Fig. 8 except we vary \mathcal{C} : $\mathcal{C} = 1$ (red), $\mathcal{C} = 0.1$ (blue). The solid curves correspond to the nonlinear dynamics at k_m [Eq. (40)] with the initial perturbation $\{\tilde{h}(0), \tilde{\Gamma}(0)\} = \{0.01, 0\}$, the dashed lines correspond to the reduced model with constant surface tension (43) with (58) with $a_0 = 0.01$, and the circles correspond to the results of numerical simulations of the original evolution equations [10].

V. CONCLUDING REMARKS

In Sec. III, we consider several different models describing the dynamics of thin liquid films. The most striking fact is that all these models describing different physical situations lead to qualitatively similar amplitude Landau equations having the form

$$\partial_2 a = -6\xi\varphi'^2(h_0)\frac{C_2}{C_c}a + \xi[\varphi''^2(h_0) + 3\varphi'(h_0)\varphi'''(h_0)]|a|^2 a, \tag{65}$$

where the multiplicative factor ξ depends on the parameters of the particular problem.

The equation (65) implies that the stability of the films is determined by a single set of conditions (47) on the body-force potential $\varphi(h)$. In the case of the unstable film, the rupture time depends on a single common factor $\varphi''^2(h_0) + 3\varphi'(h_0)\varphi'''(h_0)$ (which depends solely on the derivatives of the intermolecular potential) multiplied by a coefficient ξ depending on the model's parameters.

The reason for this similarity lies in the structure of the model equations. Computations based on the approach described in Sec. II show that the eigenvector \mathbf{U} of the linear problem proportional to the first-order solution \mathbf{u}_1 always has only one nonzero component corresponding to the thickness of the film h . Moreover, the second-order term \mathbf{u}_2 has the same structure. This means that both the tangential velocity and the surfactant concentration stationary values remain unchanged up to the second order. The nonlinear dynamics of the system reduces to that of the film thickness described by (45), so the amplitude equation coefficients structure should resemble the structure of (46). The problem-dependent factor ξ is inversely proportional to the scalar product $\mathbf{U}^\dagger \mathbf{U}$, i.e., to the coefficient of the time-derivative term in (20).

An obvious advantage of the near-critical analysis over the numerical simulation of the coupled nonlinear evolution PDE's is that the simple closed-form expression for the nonlinear rupture time (28) is available for a general van der Waals

potential. However, since the film rupture is usually governed by the fastest growing disturbance at longer wavelength with $k_m < k_c$, the estimate of the rupture time based on nearly-critical theory needs to be “tuned” by fitting the initial disturbance amplitude against the results of the numerical simulation or experiments. However, the trends of rupture time dependence on various parameters are very well captured by the near-critical theory once the amplitude of the initial disturbance is fitted at just one point in the parameter space.

We have further shown that the nonlinear analysis can be applied to the fastest growing mode via the Galerkin approximation. This mathematically less rigorous, but physically more relevant, theory yields a single amplitude equation with the coefficients in the closed form only for a one-component system, or when the decaying harmonics are entirely neglected. In general, a set of coupled amplitude equations is derived [e.g., Eqs. (63) and (64)] that can be readily integrated numerically to predict the nonlinear rupture time. This approach is still advantageous over the numerical solution of the original coupled nonlinear evolution PDEs. Galerkin's theory does not involve any adjustable parameters comparative to the near-critical theory, where the value of the initial amplitude of perturbation should be fitted and the comparison between its rupture time prediction shows an excellent agreement with the numerical results of [10] (see Figs. 8 and 9). Moreover, in cases where nonlinear stability is well described by a single amplitude equation (41) (i.e., for a one-component system, or when all the decaying modes can be dropped), the closed-form nonlinear estimate corresponding to the fastest growing mode is readily available from Eq. (43). Such an estimate, for example, was shown to accurately predict rupture time in the model of weakly slipping film on solid substrate (as in Figs. 8 and 9).

As for now, we do not have a rigorous explanation on why the near-critical theory can accurately reproduce the trends of the rupture time dependence on various parameters far from the bifurcation point upon fitting the amplitude of the initial disturbance amplitude. For a one-component system corresponding to the liquid film on solid substrate, it is, however, possible to derive the closed-form expressions for the coefficients σ_+ and κ at arbitrary $0 \leq k \leq k_c$ [see Eqs. (59) and (60)]. Comparison of the expressions for the rupture time corresponding to the near-critical theory at k_c and the fastest growing mode at k_m for the most common form of attractive potential $\varphi = \mathcal{A}/h^3$ reveals that all the parameters affect the rupture time scale to the same multiplicative factor, so there is a direct correspondence between the amplitudes of the initial disturbance [see Eq. (61)]. This finding supports the notion of the close agreement between the prediction of our near-critical theory and the results of the numerical simulation of the rupture of liquid film with insoluble surfactant [a two-component system for which a result analogous to Eq. (61) is not readily available] discussed in Sec. III D. The regions of supercritical stabilization ($\kappa < 0$) corresponding to k_c and k_m , respectively, for various types of potential (e.g., algebraic and algebraic and exponential potential) are very close in the parameter space [see Figs. 1(a) and 1(b), for example]. These findings also indicate the similarity of the perturbation dynamics in the vicinity and far from the bifurcation point, respectively. More detailed analysis will be a subject of further investigation.

ACKNOWLEDGMENTS

The authors thank Professor Richard Craster (Department of Mathematics, Imperial College) for providing the data of the numerical study of the film rupture on solid substrate from

[10] and Professor Alexander Nepomnyashchy (Department of Mathematics, Technion-IIT) for fruitful discussions. A. M. L. acknowledges the support of the Israel Science Foundation (ISF) via Grant No. 1319/09.

-
- [1] B. V. Derjaguin, *Colloid. J. USSR* **17**, 191 (1955); A. Sheludko, *Adv. Colloid Interface Sci.* **1**, 391 (1967).
- [2] A. Vrij, *Discuss. Faraday Soc.* **42**, 23 (1966); E. Ruckenstein and R. K. Jain, *J. Chem. Soc., Faraday Trans. 2* **70**, 132 (1974).
- [3] J. T. G. Overbeek, *J. Chem. Phys.* **64**, 1178 (1960).
- [4] M. B. Williams and S. H. Davis, *J. Colloid Interface Sci.* **90**, 220 (1982).
- [5] A. Oron, S. H. Davis, and S. G. Bankoff, *Rev. Mod. Phys.* **69**, 931 (1997).
- [6] J. P. Burelbach, S. G. Bankoff, and S. H. Davis, *J. Fluid Mech.* **195**, 463 (1988); R. V. Craster and O. K. Matar, *ibid.* **425**, 235 (2000).
- [7] A. De Wit, D. Gallez, and C. I. Christov, *Phys. Fluids* **6**, 3256 (1994).
- [8] O. E. Jensen and J. B. Grotberg, *J. Fluid Mech.* **240**, 259 (1992).
- [9] B. Y. Rubinstein and A. M. Leshansky, *Langmuir* **16**, 2049 (2000); B. Y. Rubinstein and S. G. Bankoff, *ibid.* **17**, 1306 (2001).
- [10] Y. L. Zhang, R. V. Craster, and O. K. Matar, *J. Colloid Interface Sci.* **264**, 160 (2003).
- [11] R. Konnur, K. Kargupta, and A. Sharma, *Phys. Rev. Lett.* **84**, 931 (2000); A. Sharma, *Eur. Phys. J. E* **12**, 397 (2003).
- [12] K. Kargupta and A. Sharma, *Phys. Rev. Lett.* **86**, 4536 (2001).
- [13] T. Erneux and S. H. Davis, *Phys. Fluids* **5**, 1117 (1993).
- [14] G. Becker, G. Grün, R. Seemann, H. Mantz, K. Jacobs, K. R. Merke, and R. Blossey, *Nature Mater.* **2**, 59 (2003).
- [15] R. Seemann, S. Herminghaus, and K. Jacobs, *Phys. Rev. Lett.* **86**, 5534 (2001).
- [16] A. Oron and S. G. Bankoff, *J. Colloid Interface Sci.* **218**, 152 (1999).
- [17] J. C.-T. Kao, A. A. Golovin, and S. H. Davis, *J. Colloid Interface Sci.* **303**, 532 (2006).
- [18] B. Y. Rubinstein and L. M. Pismen, *Int. J. Bifurcation Chaos* **9**, 983 (1999).
- [19] A. M. Leshansky and B. Y. Rubinstein, *Phys. Rev. E* **71**, 040601(R) (2005).
- [20] K. Kargupta, A. Sharma, and R. Khanna, *Langmuir* **20**, 244 (2004).